Solar Energy 204 (2020) 617–623

Contents lists available at ScienceDirect

Solar Energy

journal homepage: www.elsevier.com/locate/solener

A novel, PbS quantum dot-Sensitized solar cell structure with TiO_2-fMWCNTS nano-composite filled meso-porous anatase TiO_2 photoanode

Hamid Latif[a,*], Saima Ashraf[a], M. Shahid Rafique[b], Ayesha Imtiaz[c], Abdul Sattar[d], S. Zaheer[a], Syeda Ammara Shabbir[a], Arslan Usman[d]

[a] Department of Physics, Forman Christian College, Lahore, Pakistan
[b] Department of Physics, University of Engineering and Technology, Lahore, Pakistan
[c] Department of Chemistry, Minhaj University, Lahore, Pakistan
[d] Physics Department, COMSATS University Islamabad, Lahore Campus, Lahore, Pakistan

ARTICLE INFO

Keywords:
PbS quantum dots
TiO_2 nano rod
Quantum dot sensitized solar cell
Multiwall carbon nanotubes
Light harvesting

ABSTRACT

The research deals with fabrication of a novel quantum dot sensitized solar cells (QDSSC) architecture. Three devices, device 1, 2 and 3 with TiO_2-fMWCNTs nano composite filled meso porous anatase TiO_2 photoanodes, sensitized with PbS by 10, 15 and 20 SILAR cycles respectively were prepared. Decrease in optical band gap has been observed by increasing the SILAR cycles for PbS sensitization. QDSSC with TiO_2-fMWCNTS nano-composite filled *meso*-porous anatase TiO_2 photoanode showed a significant energy conversion efficiency of 3.8%, 5% and 5.6% for device 1, 2 and 3 respectively under the simulated light of 100 mW cm^{-2} with AM 1.5 filter. EIS analysis revealed that the device with highest power conversion efficiency has highest charge combination resistance (R_{cr}) 2852 Ω.

1. Introduction

Quantum Dots Sensitized Solar Cells (QDSSCs) are better to opt than conventional p-n junction based photovoltaic and Dye Sensitized Solar Cells because of several properties including: tunable band gap, large extinction coefficient, Multiple Exciton Generation (MEG) with single photon absorption (Tian et al., 2016; Bang and Kamat, 2010; Pedro et al., 2010; Yu et al., 2011). Quantum Dots Sensitized Solar Cells (QDSSCs) usually consist of an electrolyte sandwiched between working electrode and counter electrode. A usual photoanode of QDSSC consists of TCO glass, metal oxide particles or thin film, followed by a layer of quantum dots, while counter electrode is usually composed of Platinum, metal sulfides, carbon derivatives or conducting polymers. An electrolyte, Iodide solution, is normally sandwiched between working electrode and counter electrode to make the device work.

For an efficient QDSSC, TiO_2 particles are very good choice, to be used as metal oxide in working electrode, for the device. The main features, which make it one of the most suitable material to be used as metal oxide in QDSSC, include: phase of the crystal, surface area, pore size and desirable morphology. Meso-porous structures of anatase TiO_2 make it able to carry out high catalytic activity which is a consequence of active sites in it as well as of the large surface to volume proportion (Cui et al., 2015; Wu et al., 2014; Chen et al., 2009; Koo et al., 2008; Feng et al., 2012; Kusumawati et al., 2014; Peng et al., 2019; Dissanayake et al., 2018). Although *meso*-porous structures of anatase TiO_2 is very suitable due to its relevant propertied but lots of improvement in strength and conductivity is still required.

Since discovered, carbon nanotubes have gathered plenty of attention (Iijima, 1991). Strength is one of the properties, possessed by carbon nanotubes, which make them suitable to be used as composite. Other properties which make the tubes inevitable for several potential applications include: electrical properties i.e. conductivity, wide surface area, layered and tubular structure (Schadler et al., 1998; Dillon et al., 1997). Adsorption capacity of Carbon nanotubes is high as well as their electron conduction property (Long and Yang, 2001). TiO_2 and Carbon nanotube's composite is also a good choice to enhance the photocatalytic activity (Yu et al., 2005).

Among different component of QDSC, electron accepter is usually a wide band gap semiconductor mater (such as TiO_2) many attempts have been made to make it more efficient by introducing an electron conducting material (such as MWCNTs). Earlier 7.3% efficiency has been achieved by hydrothermally synthesized composite of TiO_2-MWCNTs based dye sensitized solar cell as compared to only 4.9% PCE of TiO_2 based solar cell thus proving that MWCNTs provide faster electron transport. (Kumar et al., 2014; Chernomordik et al., 2017; Zhao et al., 2016)

* Corresponding author.
E-mail address: hamidlatif@fccollege.edu.pk (H. Latif).

https://doi.org/10.1016/j.solener.2020.03.114
Received 16 October 2019; Received in revised form 11 March 2020; Accepted 30 March 2020

Another important component of QDSC is QDs. Near infrared (NIR) absorbing QDs like PbS or PbSe due to the possession of low bandgap energy are intensely studied and considered as a very good alternative of visible light absorbing QDs such as CdSe or CeS (Kokal et al., 2015; Huang et al., 2016; Young et al., 2016; Zhang et al., 2016). Broader spectural utilization make PbS quantum dots better sensitizer for a quantum dots sensitized solar cell which can result in better charge separation (Wang et al., 2013).

In the past few decades, quantum dots had been a subject of attention for researchers. Among various quantities, the property which make them unique from other nanomaterials is possession of quantum confinement effect (Debellis et al., 2017; Sawatsuk et al., 2009). PbS quantum dots have Bohr exciton radius of 18 nm having photo currents, approximately 20 mA/cm^2. Exciton lifetime for PbS quantum dots are 1–3 μs. In the spectral region of 300 nm-400 nm quantum dots of PbS show quantum confinement effect. Due to the possession of quantum confinement and large surface area the absorption coefficient of PbS quantum dots increases than that of bulk PbS (Lee, 2013; González-Pedro et al., 2013; Moreels et al., 2009). Another group used ZnO/PbS QD/graphene based photoanode and achieved 6.36% PCE which was higher than the PCE (5.28%) of equivalent cell without graphene (Kim et al., 2016).

In a conventional quantum dot sensitized solar cell, photoanode (working electrode) is comprised of only two layers: *meso*-porous metal oxide and quantum dots. In this work TiO_2-fMWCNTs nano-composite is used to fill the pores of the *meso*-porous anatase TiO_2 nano-rods to improve strength, conductivity and photocatalytic activity of first layer. Basic reasons, which provoke the thought of modification in the conventional working electrode, include low power conversion efficiency as well as high number of grain boundaries in TiO_2 particles (Wu et al., 2012; Fan et al., 2014). This modified *meso*-porous layer of anatase TiO_2 is sensitized by PdS quantum dots. Concentration of PbS quantum dots has been changed by 10, 15 and 20 SILAR cycles in photoanode 1, 2 and 3 respectively, to observe its effect on device efficiency. To get better efficiency, CuS thin layer has been used as counter electrode. CuS counter electrode has been proven to be better than Pt electrode. Regeneration rate of quantum dot sensitized solar cell gets remarkably enhanced due to fast S^{2-2} reduction rate (Buatong et al., 2015). To our knowledge this is the first effort to show that the TiO_2-fMWCNTs nanocomposite filled mesoporous antase TiO2 photoanode works efficiently for Quantum dot sensitized solar cells.

2. Experimental

2.1. Materials

Fluorine-doped tin oxide (FTO) coated glass (8 Ω cm^{-2}, Solarnoix), methanol (99.8%,Sigma-Aldrich), Titanium Tetraisopropoxide (TTIP) (99%, Sigma-Aldrich), Acetic Acid (HAc) (98%, Daejng), Multiwall Carbon Nanotubes (98%, Sigma-Aldrich), Concentrated Nitric Acid (99%, Daejng), Lead (ii) Nitrate (99%, Sigma-Aldrich), Thiourea (99%, Daejng), Copper (ii) Nitrate (99%, Sigma-Aldrich), Sodium Sulfide (99%, Sigma-Aldrich) are used.

2.2. Preparation of meso porus TiO_2 nano rods thin film

Under vigorous stirring, 12.5 ml of Titanium tetraisopropoxide (TTIP) was dropped in 25 ml of Acetic Acid. No precipitation was observed. 75 ml of deionized water was then added in to the solution within three minutes. Following this, solution was stirred at 50 °C for 10 h. Formation of white precipitates was observed after a few minutes of stirring, however it eventually turned clear. After completion of stirring process the obtained solution was turbid and blue gel was formed. White powder of TiO_2 was obtained by sintering of the blue gel at 500 °C for 2 h. A few drops of deionized water were added in the obtained TiO_2 powder and the mixture was grinded by ball milling. The thick paste was spread over FTO glass by doctor blade method and then was dried in oven for 30 min at 100 °C. (Cui et al., 2015)

2.3. Preparation of TiO_2-fMWCNTs (1:2) Composite:

Before formation of the composite, MWCNTs were functionalized. For functionalization and purification, 2 mg of raw MWCNTs were boiled for 30 min in 100 ml of undiluted Nitric Acid. The MWCNTs were then washed 6 times, for the removal of acid, with 150 ml of distilled water and then dried at 150 °C. 20 ml of ethanol and the functionalized MWCNTs were sonicated for 15 min. A combined solution of Titanium Tetraisopropoxide and sonicated solution of ethanol and MWCNTs (1:2) was sonicated for 30 min. The solution was sonicated for another 30 min after hydrolysis process. For 20 h, the samples were kept at 25 °C for further hydrolysis of Titanium tetraisopropoxide. The sample was then dried at 80 °C for 8 h and calcinated at 400 °C for an hour. For formation of thin film, obtained grey powder was ball milled and deposited over anatase TiO_2 covered FTO glass using doctor blade method, and then dried at 100 °C. (Yu et al., 2005)

2.4. Preparation of Lead Sulfide (PbS) quantum dots

Successive Ionic Layer Adsorption and Reaction (SILAR) cycles were used for deposition of quantum dots of PbS, as the last layer on working electrode. For device 1, the quantum dots were deposited by 10 SILAR Cycles. While for device 2 and 3, 15 and 20 SILAR Cycles were employed for the deposition of the quantum dots respectively. 0.06 M solution of $Pb(NO_3)_2$ was made using 1:1 vol ratio of methanol and deionized water as solvent while 0.3 M Thiourea solution was separately formed. The working electrode was first dipped in the $Pb(NO_3)_2$ solution and then in Thiourea solution for 60 s. For the removal of undesired ions, the FTO was dipped in ethanol for thirty seconds before and after dipping into Thiourea solution. For drying of the FTO, which by then was complete working electrode, it was kept at 100 °C for 30 min. This process was repeated to have desired SILAR Cycles (Liu et al., 2011).

2.5. Preparation of counter electrode

0.5 M solution of Cu $(NO_3)_2$ was made, using methanol as solvent. Cu $(NO_3)_2$, in methanol solution, was dropped on the FTO glass. 1 M solution of $Na_2S{\cdot}9H_2O$, in methanol and water, was dropped on the Cu $(NO_3)_2$ decorated FTO. The FTO was then rinsed with deionized water and dried with air gun and calcinated in furnace for 30 min at 450 °C (Buatong et al., 2015).

2.6. Cell assembly

To fabricate a complete quantum dot sensitized solar cell an appropriate amount of polysufied electrolyte was sandwiched between Cu_2S counter electrode and TiO_2-fmwcnts nano composite filled meso porous anatase TiO_2 photoanode. Steel clips were used to hold the cell assembly together. (See Fig. 1).

2.7. Proof of concept

There are three important factors which are important for any solar cell; first to get high power conversion efficiency, second to make the solar cell cost effective and finally to make the solar sell more stable and strong so that it can survive the effects of environment and the structure does not deteriorate over the time. In the proposed structure an effort has been made to cater all of the above three important factors.

An analogy has been shown in Fig. 2a to describe the concept behind the design of the proposed structure. Cement, sand and aggregate together are used to make concrete which has more strength as compared to its ingredients but concrete has less tensile strength. As the

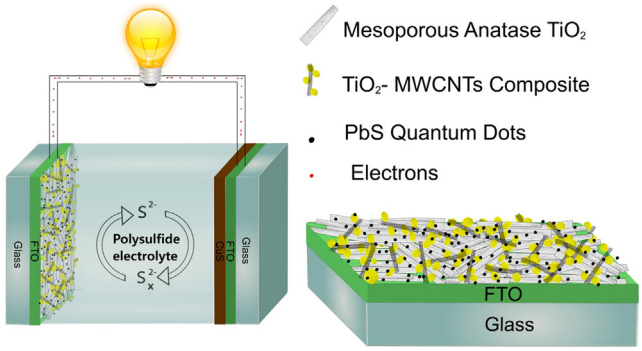

Fig. 1. Schematics of Pbs quantum dot-sensitized, solar sell structure with TiO_2-fmwcnts nano composite filled meso porous anatase TiO_2 solar cell.

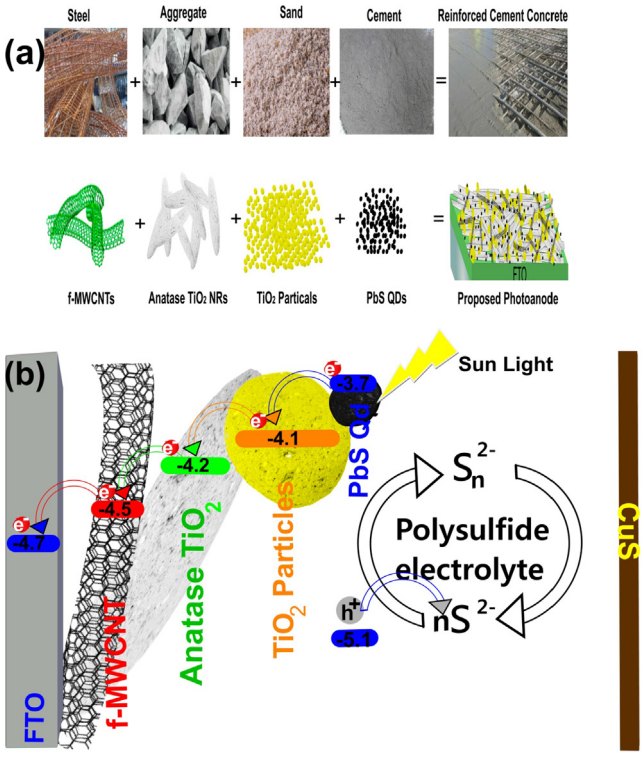

Fig. 2. (a) Design analogy for conception of the photoanode, (b) Light excitation and electron transfer depiction.

steel has higher mechanical strength, addition of steel increases the tensile strength of the cement concrete. Therefore a photoanode composed of meso porous anatase TiO_2 nano rods and TiO_2- fMWCNTs nano composite has been synthesized. Filling of meso porous anatase TiO_2 nano rods with TiO_2 nanoparticles entangled with fMWCNTs could give more strength to the photoanode. On one hand entangled fMWCNTs provide the strength to the layer on the other hand fMWCNTs embedded into TiO_2 provide effective electron transportation path as shown in Fig. 2b (Liu et al., 2012).

PbS quantum dots absorbs the visible and near to infra red light. The energy level of conduction band of TiO_2 particle is very suitable to separate the excited electron from PbS Quantum dots. The particle of TiO_2 provide more surface area as compare to the TiO_2 nano rods therefore increasing more probability of the excited electron to move to TiO_2 where as TiO_2 nano rods filed with TiO_2 nanoparticle and entangle with fMWCNTs provide additional support to separated electrons to conduct to the FTO electrode making the photoanode more efficient and strong. Moreover the materials used in the proposed device are not expensive hence making the design more efficient, strong and cost effective.

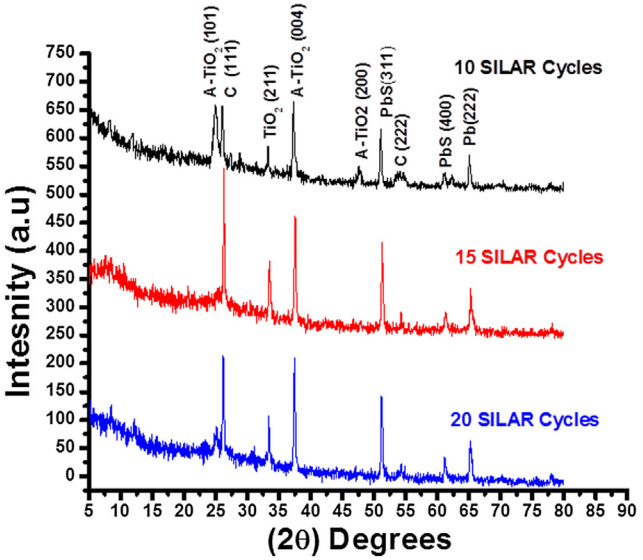

Fig. 3. XRD graph of TiO_2-fMWCNTs nano composite filled meso porous anatase TiO_2 photoanodes 1, 2 and 3 sensitized with PbS by 10, 15 and 20 SILAR cycles.

3. Results and discussion

3.1. Structural analysis

XRD patterns shown in Fig. 3 were used to analyze structure and orientation of the PbS quantum dots sensitized TiO_2-fmwcnts nano composite filled meso porous anatase TiO_2 photoanodes 1, 2 and 3 prepared with 10, 15 and 20 SILAR cycles respectively. Anatase titanium oxide (A-TiO_2) shows the diffraction peaks at 2θ of 25.2°, 37.4° and 47.7° which are indexed as crystal planes (1 0 1), (0 0 4) and (2 0 0) (Du et al., 2018; Jia et al., 2018). The obvious peaks at 2θ of 51.3°, 61.3° and 65.2° are the PbS QDs diffraction patterns with the crystal planes of (3 1 1), (4 0 0) and (2 2 2) (Li et al., 2014). A peak of TiO_2 is noticed at 33.5° with crystal plan of (2 1 1). Presence of MWCNTs was detected by peak at 26.2 with (1 1 1) crystal plan.

The peaks obtained, are shown in Fig. 3, reveals all expected phases to be present in crystalline form. TiO_2 nanoparticles in anatase form (A-TiO_2) were also obtained in all three samples. The obtained anatase peaks indicate sound crystallinity which is a consequence of slow hydrolysis and condensation of TTIP with and HAc. Another observable fact is that when compared to the template patterns, anatase TiO_2 (0 0 4) is stronger while anatase TiO_2 (2 0 0) is weaker. This observation leads to assume that the nanostructures are in rod like shapes (Cui et al., 2015). Increasing the concentration of PbS quantum dots did not significantly affect the overall peak shapes. The average crystal sizes of PbS QDs were 8, 10 and 16 nm, calculated by the Scherrer equation for 10, 15 and 20 SILAR cycles. Therefore, the average crystal size of PbS QDs has increased with the increase in SILAR cycles. The PbS QDs average crystal size resulting from SILAR methods was smaller than the PbS exciton Bohr radius of 18 nm (Zhang et al., 2017)

3.2. Morphological and topographical analysis

Morphology of PbS sensitized TiO_2-fmwcnts nano composite filled meso porous anatase TiO_2 photoanodes for 20 SILAR cycles is shown in Fig. 4 (a). Formation of TiO_2 nano rods is evident for the SEM micrograph. It can be observed that filling of Meso-Porous Anatase TiO_2 nano rods by TiO_2-fMWCNTS nano-composite is not homogeneous. Agglomeration of particles can clearly be seen in SEM micrograph. Fig. 4

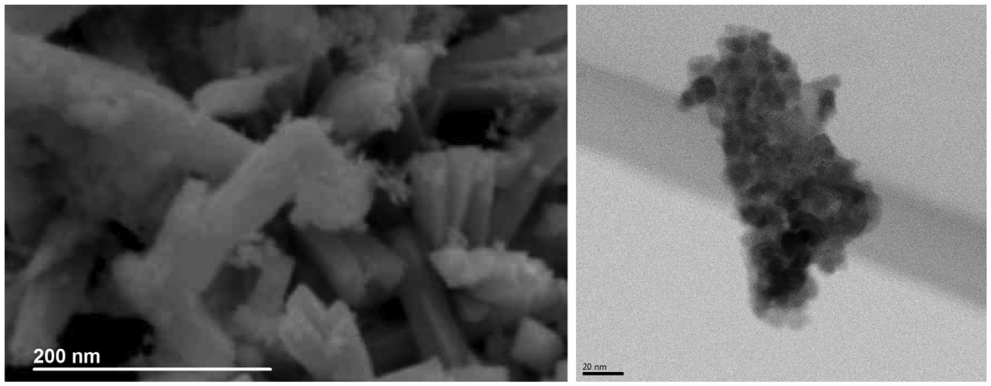

Fig. 4. (a) SEM micro graph of PbS sensitized TiO_2-fMWCNTs nano composite filled meso porous anatase TiO_2 photoanodes (b) TEM image of PbS sensitized TiO_2 nano rods.

(b) the PbS quantum dot sensitized TiO_2 nano rod. Distribution of PbS quantum dots on the nano rod is not uniform. Quantum dots are seemed to be attached with the nano rod in cluster which confirms the agglomeration of particles observed in SEM image.

Due agglomeration of nanoparticles it was difficult to find the particle size distribution there AFM three dimensional topological images were obtained and using surface profiles average size distributions of PbS quantum dots deposited at 10, 15 and 20 SILAR cycles were estimated.

Three dimensional micro images, revealing the topography and surface morphology of all three samples, along with particle size distribution graphs, obtained by the microscope can be viewed in Fig. 5.

From Fig. 5 (a, b and c) the occurrence rod like structure can clearly be seen which could be due to large growth of anatase TiO_2 (0 0 4) than anatase TiO_2 (2 0 0) which was also observed in XRD patterns. Small particles are also seemed to be attached on these rods like structures which could be identified as PbS particles.

Therefore the analysis revealed the presence of spherical particles as well as rod like structures hence confirming presence of TiO_2-fMWCNTs composite along with nanoparticles. For determine average particle size Gauss function was applied over a bar graph, which was plotted between average particle size (x-axis) and number of particles possessing the particular size (y-axis), to calculate continuous probability distribution function of the bar graph. Average particle size was highest for the sample having highest concentration of PbS quantum dots while lowest for the one having lowest concentration.

3.3. Optical absorption of photo anodes

The TiO_2-fMWCNTs nano-composite filled *meso*-porous anatase TiO_2 nano rods layer sensitized with PbS quantum dots by SILAR cycles can contribute in enhancement of light absorption by multiple scattering effects within the TiO_2 -fMWCNTs nano-composite structure and by the interfaces between *meso*-porous anatase TiO2 nano rods and TiO_2-fMWCNTs nano-composite (Dissanayake et al., 2018).

Fig. 6(a) shows the UV–Vis_NIR optical absorption spectra of photoanode 1, 2 and 3 sensitized with PbS QDs with 10, 15 and 20 SILAR cycles respectively. Each spectrum exhibits a broad absorption in the visible and near infrared (NIR) range. Optical absorption in the visible and NIR region for photoanode is increased by increasing the SILAR cycles. The absorption spectra of PbS QDs shown in Fig. 6(a) clearly indicate that QDs of PbS can harvest solar energy mainly in 900–1100 nm and a clear absorption peak can be seen at 1060 nm, 1050 nm and 1050 nm for 10, 15 and 20 SILAR cycles respectively (Zhang et al., 2017). It can be observed that the PbS QDs characteristic absorption peak for photoanode 2 is broader than characteristic absorption peaks of photoanode 1 and 3. The broadness of PbS QDs absorption peak for photoanode 2 as compare to photoanode 1 can be attributed to increase concentration of PbS QDs with increase in SILAR cycles from 10 to 15. As the concentration of PbS QDs further increases with 20 SILAR cycles the broadness of PbS QDs characteristics peaks for photoanode 3 decreases because of agglomeration of PbS QDs (Du and Tang, 2015).

Fig. 6(b) shows the plot of $(\alpha hf)^2$ versus photon energy (hf) of photoanodes 1, 2 and 3 sensitized by PbS quantum dots which can be used to find out the band gap energy of a semiconductor material where "α" is the absorption coefficient.

The calculated values of the optical band gap energy of the photoanode 1, 2 and 3 are 2.3 eV ,2.1 eV and 2.0 eV as shown in Table 1. Bandgap energy decreased by increasing concentration of PbS quantum dots. A reason for lowest bandgap energy in 3rd sample could be associated with the fact that the sample had highest particle size, which in turn could be indication of large agglomeration in the sample.

3.4. Photovoltaic performance

The graphs shown in Fig. 7 are J-V curves of solar cell with 10, 15 and 20 SILAR cycles respectively, measured under 100 mW cm^{-2} (with AM 1.5 spectral filter) condition.

All three devices have significantly high efficiency among PbS sensitized TiO_2 nano rods solar cells (Lv et al., 2019). The higher efficiency of the proposed devices with photoanode of TiO_2-fMWCNTS nano-composite filled *meso*-porous anatase TiO_2 nano rods, is attributed to multiple scattering effects within the TiO_2 -f MWCNTs nano-composite structure and also from the interfaces between *meso*-porous anatase TiO2 nano rods and TiO_2-fMWCNTs nano-composite.

From table 2 it can be seen that the power conversion efficiency has increased with increase in number of SILAR cycles**.** This behavior can be understood by observing variation of concentration of PbS quantum dots with increase in numbers of SILAR cycles. Highest power conversion efficacy of 5.6% is calculated for device 3 which is sensitized by PbS quantum dot with 20 SILAR cycles.

Highest power conversion efficiency can also be related to charge transfer at the TiO2 PbS quantum dots electrode/electrolyte interface and charge recombination at the interface of photoanone/electrolyte interface which is confirmed from the following EIS analysis.

3.5. EIS Analysis:

Electrochemical impedance spectra of each of the solar cells device were analyzed. Series resistance (R_s) and charge recombination resistance (R_{rc}) were determined by fitting the parameters with an equivalent circuit, from these data.

Fig. 8 shows the Nyquist plots of PbS quantum dots sensitized TiO_2-fmwcnts nano composite filled meso porous anatase TiO_2 nanorods at 10, 15 and 20 SILAR cycles for device 1, 2 and 3 respectively.

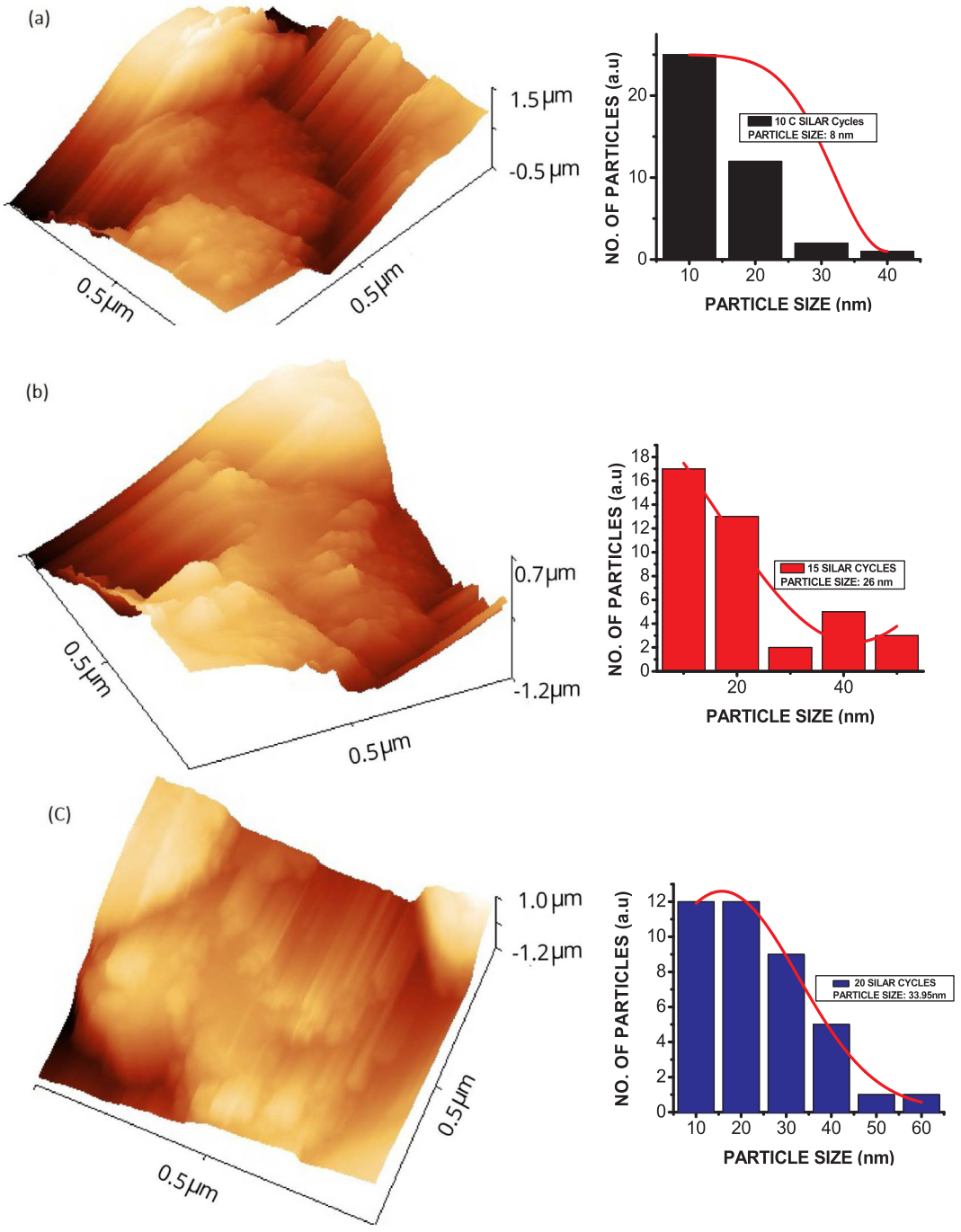

Fig. 5. (a, b and c). 3D Micro images of photoanode 1, 2 and 3 along with frequency distribution for determination of average particle size, Gaussian curve fitting is used.

R_s and R_{rc} are series resistance at FTO/TiO2 interface and recombination resistance at the photoanode/ electrolyte interface respectively. From Table 3, it can be observed that with the increase of SILAR cycles R_s value increased from 193.3 to 223.2 and 270.3. It is also evident that the R_{cr} value also increased from to 851 Ω ,1501 Ω and 2891with the increase of SILAR cycls for PbS quantum dots from 10 to 15 and 20.

Photoanode with 10 SILAR cycles shows the lowest series resistance (*Rs*) values (193.3 Ω) which leads to an efficient electron transfer at the FTO/TiO2 interface enhances the overall performance of the device 1 but the photoanode with 20 SILAR cycles exhibits the highest recombination resistance (2852 Ω) compared to the other devices. This led to reduction in recombination of the electrons in the photoanode/ electrolyte interface and enhancement in effective electron transfer which resulted in the increase in the ISC and VOC values and hence the efficiency for device 3 (Tian et al., 2014).

4. Conclusion

Three QDSSCs were fabricated, each with different concentration of PbS quantum dots. Structural analysis of photo-anodes by XRD reviled that the average crystalline size of PbS QDs was increased with increase in PbS QDs concentration. Formation of rod like structures of anatase TiO_2 was also confirmed by XRD and AFM analysis. AFM topographic

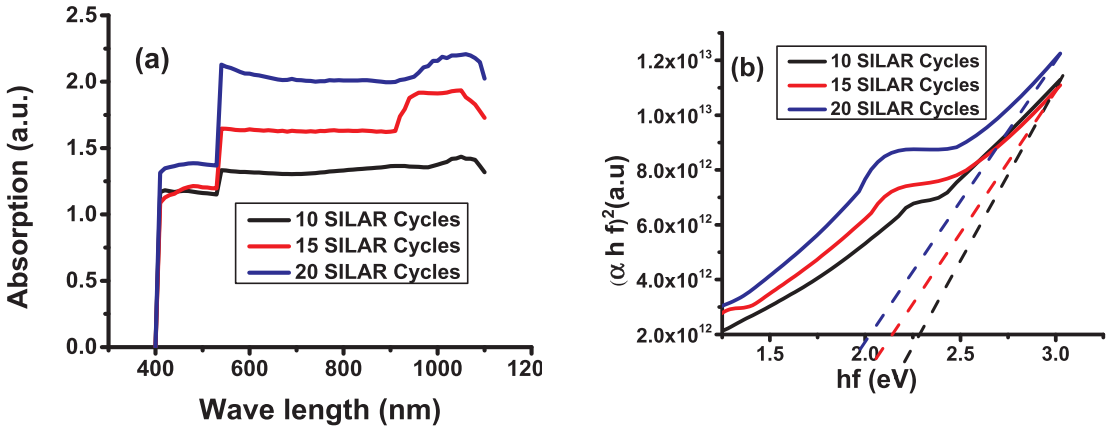

Fig. 6. (a). UV–Vis-NIR spectra and (b) $(\alpha hf)^2$ vs hf graph of photoanode 1,2 and 3.

Table 1
Optical properties of photoanode 1, 2 and 3.

SILAR cycles	Maximum absorption (a.u)	Bandgap (eV)
10	1.5	2.3
15	1.9	2.1
20	2.2	2.0

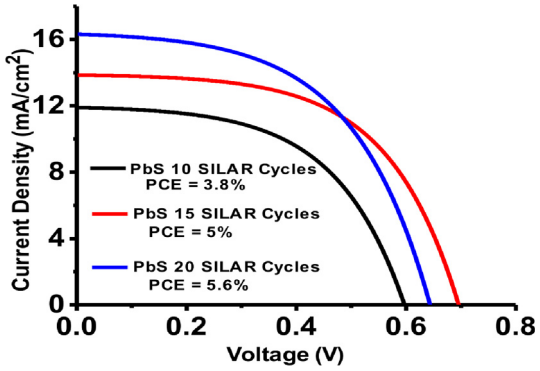

Fig. 7. J-V characterization curves for device 1, 2 and 3 decorated with PbS quantum dots by 10, 15 and 20 SILAR cycles respectively.

Table 2
Efficiency parameters List for Device 1, 2 and 3.

Device	SILAR Cycles	J_{sc} (mA)	V_{oc} (V)	V_{max} (V)	J_{max} (mA)	FF	PCE (%)
1	10	11.5	0.599	0.41	9.25	0.56	3.8
2	15	13.6	0.697	0.49	10.11	0.54	5
3	20	15.8	0.650	0.44	12.6	0.55	5.6

image reviled that average particle size of PhS QDs increased with increase of SILAR cycles which resulted in decreased in band gap calculated from UV–Visible spectroscopy analysis. The difference in concentration affected not only bandgap but also average particle size and hence efficiency. Bandgap of the three samples decreased with increased concentration of PbS quantum dots while average particle size as well as efficiency was increased with increasing concentration. The QDSSC with highest concentration of PbS quantum dots hold the highest efficiency i.e. 5.6%, attributed to lowest bandgap of 2.2 eV and highest charge combination resistance (R_{cr}) 2852 Ω.

Appendix A. Supplementary data

Supplementary data to this article can be found online at https://

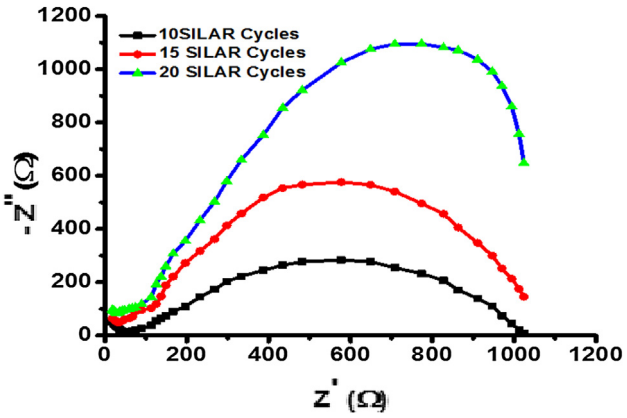

Fig. 8. Nyquist plots of PbS quantum dots sensitized TiO_2-fmwcnts nano composite filled meso porous anatase TiO_2 nanorods at 10, 15 and 20 SILAR cycles for device 1, 2 and 3 respectively.

Table 3
Charge transfer resistance and charge recombination resistance obtained by fitting the experimental spectra of PbS QD sensitized TiO_2-fmwcnts nano composite filled meso porous anatase TiO_2 nanorods solar cell at 10, 15 and 20 SILAR cycles by an equivalent circuit.

Device	SILAR cycles	Charge Transfer Resistance (R_s) (Ω)	Charge Recombination Resistance (R_{rc}) (Ω)
1	10	193.3	842
2	15	223.2	1551
3	20	270.3	2852

doi.org/10.1016/j.solener.2020.03.114.

References

Tian, J., Shen, T., Liu, X., Fei, C., Lv, L., Cao, G., 2016. Enhanced Performance of PbS-quantum-dot-sensitized Solar Cells via Optimizing Precursor Solution and Electrolytes. Sci. Rep. 6, 23094–23103.
Bang, J.H., Kamat, P.V., 2010. Solar Cells by Design: Photoelectrochemistry of TiO2 Nanorod Arrays Decorated with CdSe. Adv. Funct. Mater. 20, 1970–1976.
Pedro, V.G., Xu, X., Sero, I.M.I., Bisquert, J., 2010. Modeling High Efficiency Quantum Dot Sensitized Solar Cells. Acs. Nano. 4, 5783–5790.
Yu, X.Y., Liao, J.Y., Qiu, K.Q., Kuang, D.B., Su, C.Y., 2011. Dynamic Study of Highly Efficient CdS/CdSe Quantum Dot-Sensitized Solar Cells Fabricated by Electrodeposition. Acs Nano. 5, 9494–9500.
Cui, Y., Zhang, L., Lv, K., Zhou, G., Wang, Z.S., 2015. Low temperature preparation of TiO2 nanoparticle chains without hydrothermal treatment for highly efficient dye-sensitized solar. J. Mater. Chem. A. 3, 4477–4483.
Wu, W.Q., Xu, Y.F., Rao, H.S., Su, C.Y., Kuang, D.B., 2014. Multistack integration of three-dimensional hyperbranched anatase titania architectures for high-efficiency dye-sensitized solar cells. J. Am. Chem. Soc. 136, 6437–6445.

Chen, D., Huang, F., Cheng, Y.B., Caruso, R.A., 2009. Mesoporous Anatase TiO_2 Beads with High Surface Areas and Controllable Pore Sizes: A Superior Candidate for High-Performance Dye-Sensitized Solar Cells. Adv. Mater. 21, 2206–2210.
Koo, H.J., Kim, Y.J., Lee, Y.H., Lee, W.I., Kim, K., Park, N.-G., 2008. Nano-embossed Hollow Spherical TiO_2 as Bifunctional Material for High-Efficiency Dye-Sensitized Solar Cells. Adv. Mater. 20, 195–199.
Feng, X., Zhu, K., Frank, A.J., Grimes, C.A., Mallouk, T.A., 2012. Rapid charge transport in dye-sensitized solar cells made from vertically aligned single-crystal rutile TiO2 nanowires. Angew Chem. Int. Ed. 51, 2727–2730.
Kusumawati, Y., Hosni, M., Martoprawiro, M.A., Cassaignon, S., Pauporťe, T., 2014. Effects of Oxide Nanoparticle Size and Shape on Electronic Structure, Charge Transport, and Recombination in Dye-Sensitized Solar Cell Photoelectrodes. J. Phys. Chem. 118, 16791–16798.
Peng, Z., Liu, Z., Chen, J., Ren, Y., Li, W., Li, C., Chen, J., 2019. Influence of ZnO nano-array interlayer on the charge transfer performance of quantum dot sensitized solar cells Influence of ZnO nano-array interlayer on the charge transfer performance of quantum dot sensitized solar cells. Electrochimi. Acta. 299 216 212.
Dissanayake, M.A.K.L., Jaseetharan, T., Senadeera, G.K.R., Thotawattage, C.A., 2018. A novel, PbS: Hg quantum dot-sensitized, highly efficient solar cell structure with triple layered TiO2 photoanode. Electrochim. Acta. 269, 172–179.
Iijima, S., 1991. Helical microtubules of graphitic carbon. Nature. 354, 56–58.
Schadler, L.S., Giannaris, S.C., Ajayan, P.M., 1998. Load transfer in carbon nanotube epoxy composites. Appl. Phys. Lett. 73, 3842–3844.
Dillon, A.C., Jones, K.M., Bekkedahl, T.A., Kiang, C.H., Heben, D.S., Heben, M.J., 1997. Storage of hydrogen in single-walled carbon nanotubes. Nature. 386, 377–379.
Long, Q.R., Yang, R.T., 2001. Carbon nanotubes as superior sorbent for dioxin removal. J. American Chem. Socie. 123, 2058–2059.
Yu, Y., Yu, J.C., Yu, J.G., Kwok, Y.-C., Che, Y.K., Zhao, J.C., Ding, L., Ge, W.K., Wong, P.K., 2005. Enhancement of photocatalytic activity of mesoporous TiO2 by using carbon nanotubes. Appl. Catal. A. 289, 186–196.
Kumar, P.N., Mandal, S., Deepa, M., Srivastava, A.K., Joshi, A.G., 2014. Functionalized Graphite Platelets and Lead Sulfide Quantum Dots Enhance Solar Conversion Capability of a Titanium Dioxide/Cadmium Sulfide Assembly. J. Phys. Chem. C. 118, 18924–18937.
Chernomordik, B.D., Marshall, A.R., Pach, G.F., Luther, J.M., Beard, M.C., 2017. Quantum Dot Solar Cell Fabrication Protocols. Chem. Mater. 29, 189–198.
Zhao, T., Goodwin, E.D., Guo, J., Wang, H., Diroll, B.T., Murray, C.B., Kagan, C.R., 2016. Advanced Architecture for Colloidal PbS Quantum Dot Solar Cells Exploiting a CdSe Quantum Dot Buffer Layer. ACS Nano. 10, 9267–9273.
Kokal, Ramesh K., Naresh Kumar, P., Deepa, Melepurath, Srivastava, Avanish Kumar, 2015. Lead selenide quantum dots and carbon dots amplify solar conversion capability of a TiO 2 /CdS photoanode. J. Mater. Chem. A 3 (41), 20715–20726. https://doi.org/10.1039/C5TA04393J.
Huang, F., Zhang, L., Zhang, Q., Hou, J., Wang, H., Wang, H., Peng, S., Liu, J., Cao, G., 2016. High Efficiency CdS/CdSe Quantum Dot Sensitized Solar Cells with Two ZnSe Layers. ACS Appl. Mater. Interfaces. 8, 34482–34489.
Young, R.M., Jensen, S.C., Edme, K., Wu, Y., Krzyaniak, M.D., Vermeulen, N.A., Dale, E.J., Stoddart, J.F., Weiss, E.A., Wasielewski, M.R., Co, D.T., 2016. Ultrafast Two-Electron Transfer in a CdS Quantum Dot–Extended-Viologen Cyclophane Complex. J. Am. Chem. Soc. 138, 6163–6170.
Zhang, B., Zheng, J., Li, X., Fang, Y., Wang, L.W., Lin, Y., Pan, F., 2016. Vertically aligned ZnO/ZnTe core/shell heterostructures on an AZO substrate for improved photovoltaic performance. Chem. Commun. 52, 5706–5709.
Wang, H., Kubo, T., Nakazaki, T., Kinoshita, T., Segawa, H., 2013. PbS-Quantum-Dot-Based Heterojunction Solar Cells Utilizing ZnO Nanowires for High External Quantum Efficiency in the Near-Infrared Region. J. Phys. Chem. Lett. 4, 2455–2460.
Debellis, D., Gilgi, G., Brinck, S., Infante, I., Giansante, C., 2017. Quantum-Confined and Enhanced Optical Absorption of Colloidal PbS Quantum Dots at Wavelengths with Expected Bulk Behavior. Nano Lett. 17, 1248–1254.
Sawatsuk, T., Chindaduang, A., Kung, C.S., Pratontep, S., Tumcharern, G., 2009. Dye-sensitized solar cells based on TiO_2–MWCNTs composite electrodes: Performance improvement and their mechanisms. Diam. Relat. Mater. 18, 524–527.
Lee, J.W., 2013. Quantum-Dot-Sensitized Solar Cell with Unprecedentedly High Photocurrent. Sci. Rep. 3, 1050–1058.
González-Pedro, Victoria, Sima, Cornelia, Marzari, Gabriela, Boix, Pablo P., Giménez, Sixto, Shen, Qing, Dittrich, Thomas, Mora-Seró, Iván, 2013. High performance PbS Quantum Dot Sensitized Solar Cells exceeding 4% efficiency: the role of metal precursors in the electron injection and charge separation. Phys. Chem. Chem. Phys. 15 (33), 13835. https://doi.org/10.1039/c3cp51651b.
Moreels, I., Lambert, K., Smeets, D., Muynck, D.D., Nollet, T., Martins, J.C., Vanhaecke, F., Vantomme, A., Delerue, C., Allan, G., Hens, Z., 2009. Size Dependent Optical Properties of Colloidal PbS Quantum Dots. ACS Nano 3, 3023–3030.
Kim, B.S., Neo, D.C.J., Hou, B., Park, J.B., Cho, Y., Zhang, N., Hong, J., Pak, S., Lee, S., Sohn, J.I., Assender, H.E., Watt, A.A.R., Cha, S.N., Kim, J.M., 2016. High Performance PbS Quantum Dot/Graphene Hybrid Solar Cell with Efficient Charge Extraction. ACS Appl. Mater. Interfaces 8, 13902–13908.
Wu, W.Q., Liao, J.Y., Chen, H.Y., Yu, X.Y., Su, C.Y., Kuang, D.B., 2012. Dye-sensitized solar cells based on a double layered TiO2 photoanode consisting of hierarchical nanowire arrays and nanoparticles with greatly improved photovoltaic performance. J. Mater. Chem. 22, 18057–18062.
Fan, J., Li, Z., Zhou, W., Miao, Y., Zhanga, Y., Hu, J., Shao, G., 2014. Dye-sensitized solar cells based on TiO2 nanoparticles/nanobelts double-layered film with improved photovoltaic performance. Appl. Surf. Sci. 319, 75–82.
Buatong, N., Tang, I.M., On, W.P., 2015. Quantum dot-sensitized solar cells having 3D-TiO2 flower-like structures on the surface of titania nanorods with CuS counter electrode. Nanoscale Res. Lett. 146–156.
Liu, C., Liu, Z., Li, Y., Ya, J., An, L.E.L., 2011. CdS/PbS cosensitized ZnO nanorods and its photovoltaic properties. Appl. Surf. Sci. 257, 7041–7046.
Liu, X., Wang, C., Cai, B., Xiao, X., Guo, S., Fan, Z., Li, J., Duan, X., Liao, L., 2012. Rational Design of Amorphous Indium Zinc Oxide/Carbon Nanotube Hybrid Film for Unique erformance Transistors. Nano Lett. 12, 3596–3601.
Du, K., Liu, G., Chen, X., Wang, K., 2018. Fast charge separation and photocurrent enhancement on black TiO2 nanotubes cosensitized with Au nanoparticles and PbS quantum dots. Electrochim. Acta 277, 244–254.
Jia, J., Mu, L., Lin, Y., Zhou, X., 2018. Rutile versus anatase for quantum dot sensitized solar cell. Electrochim. Acta 266, 103–109.
Li, X., Lu, W., Wang, Y., Fang, Y., Wang, L., Ai, Q., Zhou, X., Lin, Y., 2014. Pre-synthesized monodisperse PbS quantum dotssensitized solar cells. Electrochim. Acta 144, 71–75.
Zhang, Z., Shia, C., Xiaoa, G., Lv, K., Ma, C., Yue, J., 2017. All-solid-state quantum-dot-sensitized solar cells with compact PbS quantum-dot thin films and TiO_2 nanorod arrays. Ceramics Intern. 43, 10052–10056.
Du, M., Tang, G.H., 2015. Optical property of nanofluids with particle agglomeration. Solar Energy. 122, 864–872.
Lv, K., Shi, C., Ma, C., Wang, Q., Chen, W., 2019. Introduction of polysulfide anions to increase the loading quantity of PbS quantum-dots for efficient solid-state quantum-dot sensitized TiO2 nanorod array solar cells. J Nanopart Res. 21, 2–8.
J. Tian, L. Lv, C. Fei, Y. Wang, X. Liua, G. Cao, A highly efficient (> 6%) Cd1-xMnxSe quantum dot-sensitized solar cell, J. Mater. Chem. A 2(2014) 19653.